9734 *Biochemistry* **2009,** *48,* 9734–9744
DOI: 10.1021/bi900556a

BIOCHEMISTRY
including biophysical chemistry & molecular biology
Article

The Stathmin-Derived I19L Peptide Interacts with FtsZ and Alters Its Bundling[†]

Marie-Jeanne Clément,[‡] Boi-trinh Kuoch,[‡] Tap Ha-Duong,[§] Vandana Joshi,[‡] Loic Hamon,[‡] Flavio Toma,[‡] Patrick A. Curmi,*[,‡] and Philippe Savarin*[,‡]

[‡]*Laboratoire Structure-Activité des Biomolécules Normales et Pathologiques, INSERM/UEVE U829, Evry, 91025 France, and* [§]*Laboratoire Analyse et Modélisation pour la Biologie et l'Environnement, UMR/UEVE 8587, Evry, 91025 France*

Received April 2, 2009; Revised Manuscript Received September 7, 2009

ABSTRACT: FtsZ is a prokaryotic tubulin-like protein. Despite a low degree of sequence identity with tubulin, it presents the same folding pattern and some similar functions, notably in cell division. Indeed, FtsZ and tubulin polymerize to form bundles and microtubules, respectively, which are essential for cell cytokinesis. We previously demonstrated that peptides derived from the N-terminal stathmin domain interact with tubulin and impede microtubule formation. We demonstrated here that I19L, the most efficient of these peptides, also alters FtsZ bundling assembly in vitro. STD-NMR and TRNOESY experiments revealed that I19L interacts with FtsZ and folds upon its binding but in a way different from what we observed with tubulin. These NMR data were used in molecular modeling calculations to propose models of the I19L−FtsZ complex. Interestingly, two models, consistent with NMR data, show an interaction of I19L near the T7 loop or near the GTP binding site of FtsZ, explaining the modifications of the bundling assembly observed with this peptide. The fine analysis of the structural differences of the complexes of I19L with FtsZ and tubulin should help for the rational development of new specific antibiotic agents.

FtsZ is one of the major proteins implicated in cell division in bacteria (*1*). The FtsZ protein is implicated in the formation of the Z-ring, which determines the site of cytokinesis and appears to be a good candidate for discovering new antibiotics agents (*2*).

FtsZ contains two domains arranged around a central helix; the first domain corresponds to a GTPase domain, and the other, the carboxy-terminal domain, is a four-stranded β sheet tilted by 90° against the β sheet of the GTPase domain (*3*).

The $\alpha\beta$-tubulin protein is the building block of microtubules in eukaryotes. Microtubules are major components of the eukaryotic cytoskeleton and are implicated in various critical functions such as cell division, motility, and intracellular trafficking. Despite a low degree of sequence identity (< 20%), the structures of FtsZ and of α- or β-tubulin are highly homologous (*3*, *4*), and both proteins play an essential role in cell division. However, some remarkable differences exist between these two proteins. In contrast to tubulin, FtsZ is monomeric and does not assemble into cylindrical polymers (like microtubules) but rather forms filaments which also do not present a dynamic instability behavior as observed for microtubules (*5*). The GTP binding pocket of FtsZ is formed by helices H1−H6 and strands S1−S6. Loops T1−T6 are part of this pocket on one side of the molecule. Loop T7 is in the C-terminal domain and is involved in the longitudinal interactions between subunits and involved in the nucleotide hydrolysis process (*6*). In contrast to microtubules where the nucleotide-binding pocket is occluded, the nucleotide remains exchangeable in FtsZ protofilaments (*7*). Interestingly, some mutations in the T7 loop of FtsZ severely affect FtsZ polymerization and GTP hydrolysis (*8*), which underline its role in the regulation of FtsZ activity.

Numerous studies have addressed the interaction between different kinds of drugs and tubulin or FtsZ polymers. Among the drugs used in clinical applications, paclitaxels (*9*) and peloruside (*10*), epothilones (*11*) bind with higher affinity to polymerized tubulin than to soluble tubulin and stabilize microtubules. The second class concerns molecules that bind preferentially to tubulin and promote microtubule disassembly. Vinblastine, vincristine, the semisynthetic analogues vinflunine and vinorelbine, and two antimitotic peptides phomopsin A and soblidotin (*12*) bind to the vinca domain on tubulin. This domain is located adjacent to the exchangeable GTP-binding pocket on β-tubulin at the plus end (+) longitudinal interface (*13*). Finally, the colchicine binding site is located at the intradimer interface between α-tubulin and β-tubulin (*14*). In the case of FtsZ, drugs bind either to the GTP pocket (*15*) or to the T7 loop as cinnamaldehyde (*16*). Recently, PC190723 has been proposed to bind to a region analoguous to the paclitaxel binding site of tubulin (*17*). According to the great degree of structural similarity between FtsZ and tubulin, some ligands have been found to act on both proteins: bis-ANS (*18*) and sanguinarine (*19*, *20*). Some compounds have a different impact on tubulin and FtsZ polymers. For example, calcium induces the formation of FtsZ bundles (*21*) but inhibits tubulin polymerization (*22*). Glutamate increases the GTPase activity in tubulin (*23*) but strongly suppresses this activity for FtsZ (*24*). Differences in the nucleotide binding site may also explain why some C8-substituted GTP analogues could inhibit FtsZ polymerization but have an opposite effect on tubulin polymerization (*25*). Interestingly, most of the

[†]This work was supported by Institut National de la Santé Et de la Recherche Médicale, Association pour la Recherche sur le Cancer (ARC). The Région Ile de France, the Conseil Général de l'Essonne, Genopole, DSV/CEA, and the Association Française de lutte contre la Myopathie (AFM) are acknowledged for their contribution to the NMR equipment.

*To whom correspondence should be addressed: Laboratoire Structure-Activité des Biomolécules Normales et Pathologiques, INSERM/UEVE U829, Evry, 91025 France. Telephone: (33) 1 69 47 03 23. Fax: (33) 1 69 47 02 19. E-mail: philippe.savarin@univ-evry.fr or pcurmi@univ-evry.fr.

 Published on Web 09/10/2009

tubulin targeting agents, including paclitaxel, vinblastine, and colchicine, do not affect FtsZ assembly dynamics (*18*).

With regard to the tubulin protein partners, MAPs or tau bind with higher affinity and stabilize microtubules, usually through the C-tail of tubulin. On the other hand, the structure of the stahmin:tubulin complex showed that stathmin forms a T_2S complex through extensive interaction with tubulin, excluding its C-terminus (*14*). In the same way, FtsZ protein partners have been shown to mainly bind on the C-terminal tail as FtsA (*26*), ZipA (*27*, *28*), recently EzrA (*29*), or SepF (*29*). Other sites remain putative. YlmF could interact with the C-terminus of FtsZ (*30*) while MciZ could bind to the GTP pocket of FtsZ (*31*). For some protein partners of FtsZ, the binding site remains unknown as for the interaction between ZapA or YgfE, one of its orthologues. The C-terminus of MinC has recently been demonstrated to prevent FtsZ−FtsZ lateral interactions, while its N-terminal domain lowers the rigidity of FtsZ filaments, through an unknown mechanism (*32*). Finally, only one inhibitor, SulA, has been found to fix on the T7 loop (*33*).

I19L is a short peptide derived from the N-terminal part of stathmin. We have previously shown that this peptide interacts with tubulin and impedes microtubule formation (*34*). Here, we addressed the possibility that I19L could also influence FtsZ polymerization because of structural similarities between FtsZ and tubulin.

We demonstrate a direct interaction between I19L and FtsZ. Thus, we discovered a peptide able to interfere with both microtubule and FtsZ bundling assembly. Models of I19L−FtsZ complexes, derived from the combination of NMR data and docking calculations, allowed us to characterize the differences in the interaction of I19L with FtsZ and tubulin. The results open new possibilities for developing original new small drug candidates acting specifically on FtsZ.

MATERIALS AND METHODS

FtsZ Purification. *Escherichia coli* FtsZ was purified as described previously (*35*) with some modifications. Briefly, FtsZ was overexpressed in *E. coli* strain BL21-DE3. Cells were harvested by centrifugation (4000*g* for 10 min), and pellets were resuspended in 25 mM Pipes (pH 6.7), 10 mM $MgCl_2$, and 50 mM KCl (PEM buffer) before being lysed on ice using a sonicator. The soluble fraction was separated from the cell debris by centrifugation 100000*g* for 1 h. The protein was extracted via one cycle of Ca^{2+}- and glutamate-induced precipitation; 1 mM GTP, 20 mM $CaCl_2$, and 1 M glutamate were added after 10 min at 37 °C to the solution. The pellet (50000*g* for 15 min), which contains FtsZ, was resuspended in 10 mL of PEM buffer and centrifuged for 15 min at 12000*g* and 4 °C.

Peptides. The I19L peptide was synthesized by Epytop (Nîmes, France) using Fmoc [*N*-(9-fluorenyl)methoxycarbonyl] chemistry. The purity and integrity of the peptide were verified by mass spectrometry. The peptide was dissolved in water with the help of NH_4OH vapors.

Protein Quantification. The concentration of FtsZ was measured by the Bradford method using BSA as a standard (ratio of absorbance of EcFtsZ to absorbance of BSA equal to 0.82) (*36*).

AFM Imaging. Five minutes after the onset of FtsZ polymerization at 37 °C, freshly cleaved mica was dipped in the solution. Mica was removed from the mixture, plunged into a 0.02% (w/v) uranyl acetate solution to maintain the conformation of FtsZ, rinsed in pure water, and dried with filter paper.

Imaging was performed in tapping mode with a Multimode AFM (Veeco, Santa Barbara, CA) operating with a Nanoscope IIIa controller. We used Olympus (Hamburg, Germany) AC160TS silicon cantilevers with nominal spring constants of 36−75 N/m. The scan frequency was typically 1.5 Hz per line; the modulation amplitude was a few nanometers, and the *z* scale was from 10 to 30 nm.

In Vitro FtsZ Polymerization Assay. FtsZ (or FtsZ mixed with I19L at different concentrations) was dissolved at a concentration of 10 μM in PEMC buffer (PEM containing 10 mM $CaCl_2$ and 1 mM GTP) in a final volume of 120 μL. The dynamics of FtsZ assembly was monitored by 90° light scattering at 350 nm in a PTI QuantaMaster 2000-4 thermostated spectrometer at 37 °C (1 cm light path).

FtsZ Sedimentation Assay. FtsZ (or FtsZ mixed with 200 μM I19L) was added at a concentration of 12 μM to PEM buffer in the presence of GTP (1 mM). Calcium was finally added up to a concentration of 10 mM. The samples (100 μL) were polymerized for 5 min at 37 °C and ultracentrifuged at 700000*g* for 30 min or 25000*g* for 15 min. The pellets were resuspended in 50 μL of PEM buffer, and 20 μL was loaded on a 12% SDS−PAGE gel for analysis.

NMR Spectroscopy. All ^{1}H NMR experiments were performed at 293 K on a Bruker Avance 600 MHz NMR spectrometer equipped with a cryoprobe. Data were processed using Topspin (Bruker). Sodium [3-trimethylsilyl-2,2′,3,3′-$^2H_4$]-propionate (TSP-d_4) was used as an internal reference for proton chemical shifts.

Spectra of I19L (when free) were collected at a peptide concentration of 1 mM in a H_2O/D_2O (90:10) mixture at pH 6.8. The NMR sample of I19L in interaction with FtsZ contained 1 mM peptide and 20 μM FtsZ, with a 50:1 peptide:protein molar ratio, in 50 mM sodium phosphate buffer (pH 6.8), containing 0.02% NaN_3 and 10% D_2O. To detect nonspecific interactions, a control sample was prepared in a similar way but FtsZ was replaced with bovine serum albumin (BSA). One-dimensional (1D) proton spectra were recorded with 64 scans and 16K data points. For sequence-specific assignments, two-dimensional (2D) DQF-COSY (*37*), TOCSY (*38*), NOESY (*39*), and ROESY (*40*) spectra were used. The TOCSY experiments were acquired using the MLEV17 sequence (*41*) with a mixing time of 80 ms. In the NOESY and TRNOESY experiments (*42*, *43*), the mixing period was 200 ms. A mixing time of 100 ms was used to verify that spin diffusion is limited. The 2D ROESY spectrum was recorded with a mixing time of 300 ms. All 2D experiments were conducted with 2048 data points × 512 increments × 64 scans with a spectral width of 6000 Hz in both dimensions. The data were zero-filled to give a 4096 × 1024 data matrix prior to Fourier transformation. One-dimensional STD-NMR experiments (*44*) with I19L interacting with FtsZ were conducted with 1024 scans. The protein resonances were saturated at −1 or 0 or 10 ppm (40 ppm for reference spectra) with a cascade of 40 selective Gaussian-shaped pulses 50 ms in duration, with a 1 ms delay between each pulse, resulting in a total saturation time of 2.04 s. Subtraction of saturated spectra from reference spectra was performed by phase cycling. In all experiments, suppression of the water signal was achieved with the WATERGATE sequence before acquisition (*45*). The NMR spectra were visualized and analyzed with NMRView version 5.0.4 (*46*).

Structure Calculations. Distance constraints for structure calculations were derived from the 200 ms mixing time TRNOESY spectrum. The volumes of the NOESY cross-peaks

were measured with NMRView and converted to distances using the relationship $I_{ij}/I_{ref} = (r_{ref}/r_{ij})^6$ (*47*) using the distance between the Phe 15 Hβ protons (1.74 Å) as a reference. An error of ±20% was applied for all distances. According to the observed long-range effects for residues 3, 4, 6, 7, 13, 14, and 17, the corresponding ϕ angles appeared during the first runs with CNS 1.1 (*48*) in the Ramachandran β sheet zone. These ϕ angles were enforced ($-90 \pm 40°$) in the final run without being violated. A total of 400 structures were calculated using a standard simulated annealing protocol. Of these calculated structures, the quality of the 40 structures with lower total energy was analyzed with PROCHECK version 3.5.4 (*49*) and visualized with MOLMOL version 2.6 (*50*).

Docking Calculations. To propose a model of I19L in interaction with FtsZ, the lowest-total energy structure of I19L was used to perform docking calculations with FtsZ. The calculations were conducted using the coarse-grained protein model recently developed by Basdevant et al. (*51*). The simplified model describes each amino acid backbone with one bead and the side chains with one or two other grains, depending on their size. This coarse-grained description at the residue scale, in combination with a multiminimization procedure (see below), has been shown to efficiently predict the quaternary structure of protein−protein complexes (*52*). The Van der Waals potentials and the partial charges of the coarse grains were derived from the all-atom second-generation AMBER force field (*53*). The coarse-grained model has been shown to provide an efficient discriminating scoring energy function for the protein−protein docking problem. It has allowed recovery of the experimentally known quaternary structure of several protein−protein complexes, including the trypsin−BPTI and the barnase−barstar complexes (*51*).

The docking procedure begins with generation of initial conformations of the complex with quasi-exhaustive different positions and orientations of I19L relative to FtsZ. Each configuration is created so that the intermolecular distance between the closest coarse grains is adjusted to 4 Å. The two latitude and longitude angles that characterize the position and the three Euler angles that described the orientation are sampled regularly with an incremental angle of 30°. Then the 46128 generated complexes are minimized in energy using a conjugate gradient algorithm. A simple sigmoidal distance-dependent dielectric function was used to implicitly model the solvent screening effect of electrostatic interactions (*54*). No explicit water model is included in the minimization procedure. The reliability of the method has again been tested on the docking of I19L to the α-tubulin monomer (data not shown).

I19L was thus docked with two different FtsZ structures. The first one (denoted FtsZw) is the experimental structure 2VAP from *Methanococcus jannaschii* which has a resolution of 1.7 Å. The GDP was not considered, and we limited the protein to the K39−G339 sequence, which is the globular part of the FtsZ structure. Because the model does not yet include the possible large conformational changes of protein loops, I19L was also docked to a deleted FtsZ (denoted FtsZd) in which residues G230−V234 of loop T7 (loop also existing in tubulin which moves upon binding of I19L) have been deleted, to test whether I19L can bind to this site, when the T7 loop moves apart from it. The absence of the loop's flexibility in the model is clearly a drawback in our approach. However, in the case of the docking of known bound structures or quasi-rigid molecules, the method allows us to acquire useful information about their possible interactions that can help structure resolutions. A possible way to improve the predictions is to perform several docking calculations using different conformations of the protein loops. This would be, however, much more computationally expensive and time-consuming, so we have preferred to simply delete the T7 loop to yield a rapid insight into possible interactions of I19L with this part of FtsZ.

RESULTS

I19L Disturbs FtsZ Bundling Assembly. The quality of FtsZ production and purification was certified by AFM imaging under conditions of filament assembly in the presence of GTP and bundling in the presence of calcium (Figure 1A,B). The effect of I19L on FtsZ (10 μM) polymerization was then analyzed by 90° light scattering and sedimentation assays at 37 °C in the presence of 10 mM $CaCl_2$. We observed that, compared to the control, the presence of I19L reduced the steady state plateau value in a concentration-dependent manner (Figure 1C). As light scattering data reflect both polymerization and bundling, we attempted to discriminate a putative interaction of I19L with either FtsZ filaments or thick bundles. The sample was thus centrifuged at high speed (700000*g* for 30 min) in the presence of GTP, calcium, and 200 μM I19L to detect interaction of I19L with both protofilaments and bundles (Figure 1D). We found that I19L coprecipitates with FtsZ protofilaments and bundles with no effect on the total mass of FtsZ polymers. A parallel low-speed centrifugation (25000*g* for 15 min) was used to separate FtsZ filaments from thick bundles (Figure 1D). Under these conditions, I19L was found in the pellet, which indicated an interaction of I19L with FtsZ bundles. Interestingly, the amount of FtsZ in the pellet is increased in the presence of I19L, suggesting that I19L promotes the formation of large bundles.

I19L Interacts with FtsZ via Hydrophobic Residues. We showed previously by NMR and circular dichroism that I19L is mostly disordered in solution (*34*) and adopts a β hairpin conformation when in contact with tubulin. We evaluated here the molecular interaction of I19L with FtsZ by different NMR methods. We first probed the protons of I19L in interaction with FtsZ by 1D STD-NMR using a 30:1 I19L:FtsZ molar ratio. During the 1D STD-NMR experiments, the resonances of FtsZ were saturated at 0, −1, or 10 ppm where no I19L resonances are present (Figure 2 and Figure S1 of the Supporting Information). These 1D STD-NMR spectra first clearly show an interaction of I19L with FtsZ in agreement with the results obtained from the light scattering and the sedimentation experiments. Furthermore, the STD-NMR data allowed us to point out protons of I19L in contact with FtsZ. We found that the aromatic protons of F15 and the hydrophobic side chains of L6, L17 and/or L19, and I1 are in close contact with FtsZ, describing the interaction zone of I19L with FtsZ.

Determination of the Structure of I19L Bound to FtsZ. The structure of I19L in interaction with FtsZ was investigated using 2D transferred nuclear Overhauser effect spectroscopy (TRNOESY). The TRNOESY spectrum of I19L in the presence of FtsZ confirmed the interaction between these two molecules and suggests that I19L folds in contact with FtsZ (Figure 3B). Some negative cross-peaks appeared in the aromatic region, and the analysis of the spectrum showed some long- and medium-range NOEs (Table 1) that reflect a folding of the peptide upon binding to FtsZ.

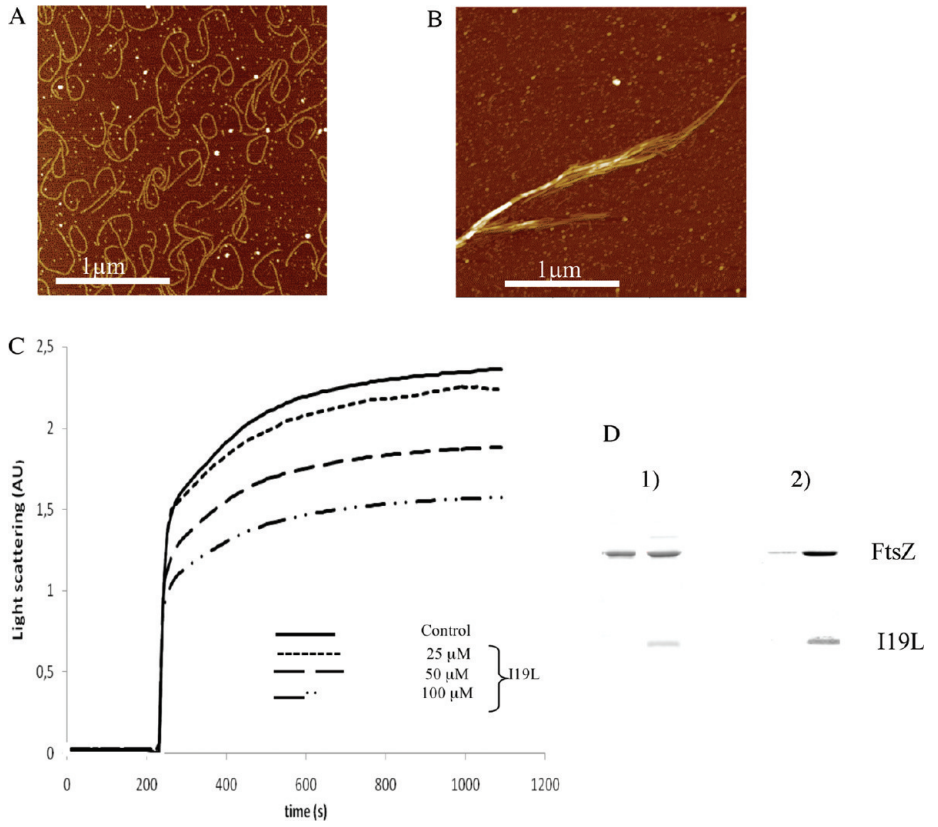

FIGURE 1: (A) AFM imaging of FtsZ assembly in the absence of calcium. FtsZ (5 μM) was assembled at 37 °C in PEM buffer [25 mM Pipes (pH 6.7), 10 mM $MgCl_2$] and 1 mM GTP as previously described (*63*). The incubation time was 60 s. The *z* scale was 10 nm. (B) Visualization of FtsZ bundles by AFM. FtsZ (10 μM) was assembled at 37 °C in PEMC buffer [25 mM Pipes (pH 6.7), 10 mM $MgCl_2$, 10 mM $CaCl_2$, and 1 mM GTP]. The incubation time was 5 min, and the *z* scale was 30 nm. (C) I19L alters FtsZ assembly in the presence of calcium. FtsZ (10 μM) was assembled under control conditions at 37 °C in PEMC buffer [25 mM Pipes (pH 6.7), 10 mM $MgCl_2$, 1 mM GTP, and 10 mM $CaCl_2$] or with varying concentrations of I19L. (D) I19L cosediments mainly with FtsZ bundles. (1) SDS−PAGE of high-speed centrifugation pellets of steady state FtsZ polymers formed at 12 μM in the presence of calcium under control conditions (left) or in the presence of 200 μM I19L (right) (700000*g* for 30 min). (2) SDS−PAGE of low-speed centrifugation pellets of steady state FtsZ polymers formed at 12 μM in the presence of calcium under control conditions (left) or in the presence of 200 μM I19L (right) (25000*g* for 15 min).

To assess the specificity of these cross-peaks, similar TRNOESY experiments were undertaken with I19L and BSA instead of FtsZ as a nonspecific target. The differences between I19L TRNOESY spectra in the presence of FtsZ and BSA helped us to unravel the specific cross-peaks. We finally compared the TRNOESY spectrum of I19L obtained in the presence of FtsZ with that obtained with tubulin. Some differences were observed between those spectra that indicate that the structure of I19L is different when in interaction with FtsZ or tubulin (Figures 3B,C and 4).

Description of the I19L Structure. An analysis of the structures shows that no residues have a ϕ or ψ dihedral angle in the bad regions of the Ramachandran plot with no violation larger than 1 Å. The root-mean-square deviation (rmsd) of the mean structure for these structures on the backbone is 0.91 Å. The number of TRNOEs used was particularly important (245, which represents 12.9 nOes per residue), which helped us to obtain a high resolution of the structure. Fifteen long-range nOes were observed between residues 2 and 18, residues 3 and 17, residues 5 and 16, residues 6 and 15, and residues 8 and 13 that participate in the fold of this peptide. The dispersion of the lateral chain of I1, R9, and L19 probably reflects the high flexibility of these residues (Figure 5). Zero inter-residue nOes, three inter-residue nOes, and one inter-residue nOe are found between the lateral chains of I1, R9, and L19, respectively. One bend was observed between residues 9 and 12. Residues 2−6 and 12−18 have repetitive ϕ and ψ values falling into the β region of the Ramachandran map and characteristic of isolated extended strands (*55*). Hydrogen bonds have been calculated with MOLMOL. Two H-bonds were observed between the backbone of K4 and E16. Salt bridges are observed between the lateral chains of residues 8−13 and 4−16, as observed previously for other isolated extended strands (*55*). Interstrand hydrophobic interactions (I1−L19, F15−L6, F15−L17, and L17−V3) participate in the stabilization of the structure.

Two Different Binding Sites of I19L on FtsZ Are Consistent with NMR Data. To identify the binding site of I19L on FtsZ, docking calculations were performed. The eight lowest-energy structures of I19L−FtsZw and I19L−FtsZd complexes obtained are listed in Table 2. The table also shows the number of occurrences for each structure, as well as the average of the minimal distances between peptide residues I1, L6, F15, L17, and L19 and FtsZ.

In the first seven lowest-energy structures of the I19L−FtsZw complex, the peptide is located in the GTP pocket of the protein. Docking positions differ only in their relative orientations. In the eighth structure, I19L interacts and is aligned along with the long central helix H7 that separates the two FtsZ subdomains. Among these eight conformations, the fifth and seventh ones are the most populated and are displayed in Figure 6. When I19L is docked with FtsZd, which has a partially deleted loop T7, the binding sites of the first, third, fourth, fifth, and sixth lowest-energy

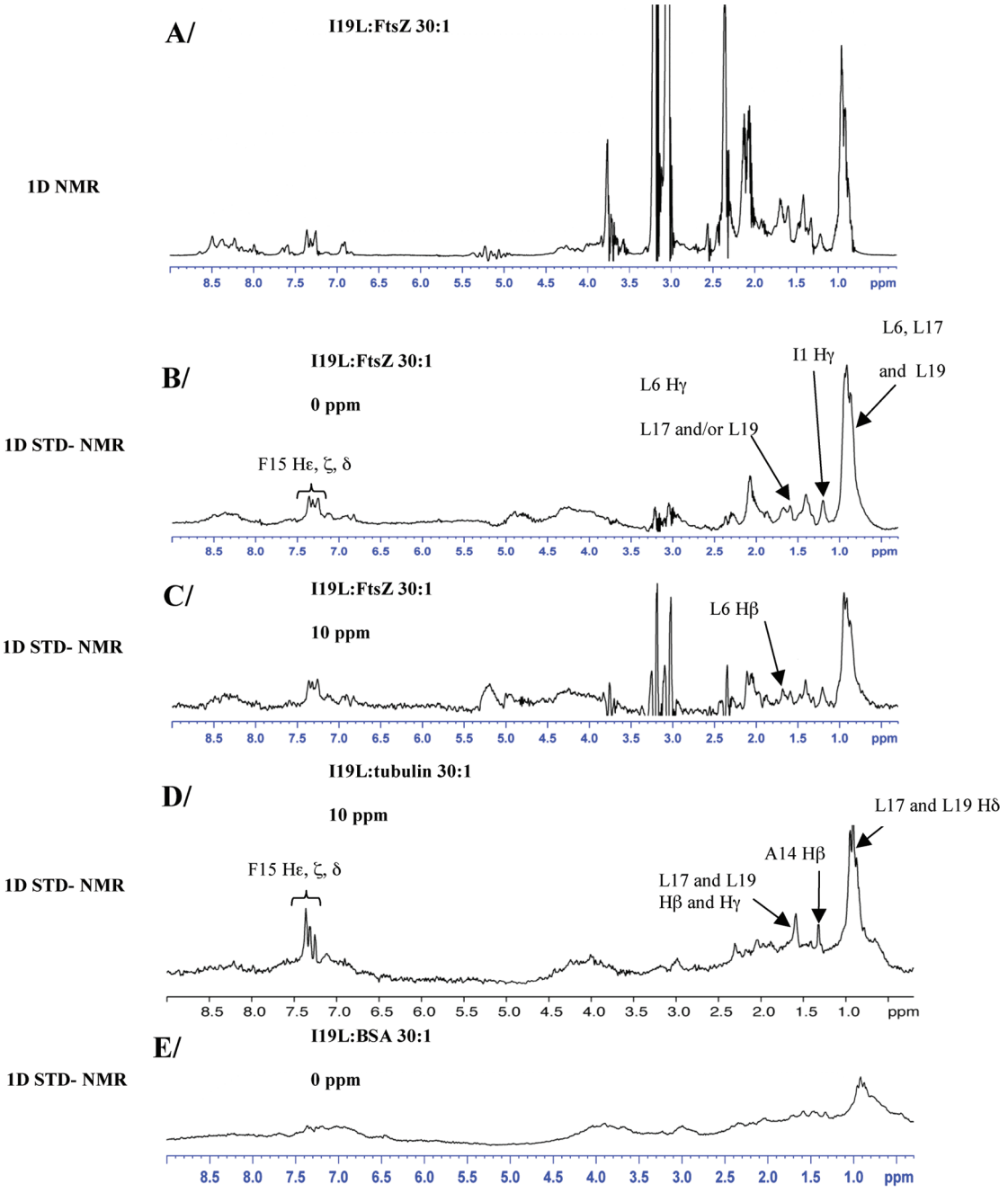

FIGURE 2: I19L interacts specifically with FtsZ and tubulin. 1D NMR spectra of 1 mM I19L at 20 °C in the presence of (A) 30 μM FtsZ, (B) 30 μM FtsZ with selective saturation of protein resonances at 0 ppm, (C) 30 μM FtsZ with selective saturation of protein resonances at 10 ppm, (D) 30 μM tubulin with selective saturation of protein resonances at 0 ppm, and (E) 30 μM BSA with selective saturation of protein resonances at 0 ppm, demonstrating the specificity of I19L−FtsZ and I19L−tubulin interactions.

structures are also located in the GTP pocket. However, in the second, seventh, and eight conformations, I19L interacts with the β sheet of the C-terminal domain, exactly at the position occupied by the T7 loop in the wild-type protein (Figure 6).

These theoretical results were combined with the experimental NMR observations to determine the most probable structure of the I19L−FtsZ complex. Among the lowest-energy structures of I19L bound to FtsZw, the second and seventh ones are the complexes for which the protein−ligand averaged minimal distance is the shortest and in which I19L residues I1, L6, F15, L17, and L19 are clearly in close contact with FtsZ, as observed by the STD-NMR experiments. In the fifth I19L−FtsZw structure, which has been found most frequently, the distances from the residues I1, L6, F15, and L17 to the protein are ~5 Å, whereas the distance from residue L19 is greater than 11 Å (see Table 1 of the Supporting Information). Because it is not clear from NMR experiments whether both L17 and L19 residues or only one of them interact with FtsZ, this fifth complex conformation cannot be excluded from the most probable structures. In these similar conformations, I19L is positioned at the same location but is oriented in a different direction (Figure 6). As indicated in Table 2 by arrows, five of the lowest-energy structures of the I19L−FtsZd complex correspond to structures found when docking I19L to FtsZw, in which the peptide is located in the GTP pocket. In the seventh structure, I19L lies perpendicular to the β-sheet of the C-terminal domain and between starting residues H8 and H10 of the α-helices, occupying exactly the same place as the deleted T7 loop. For

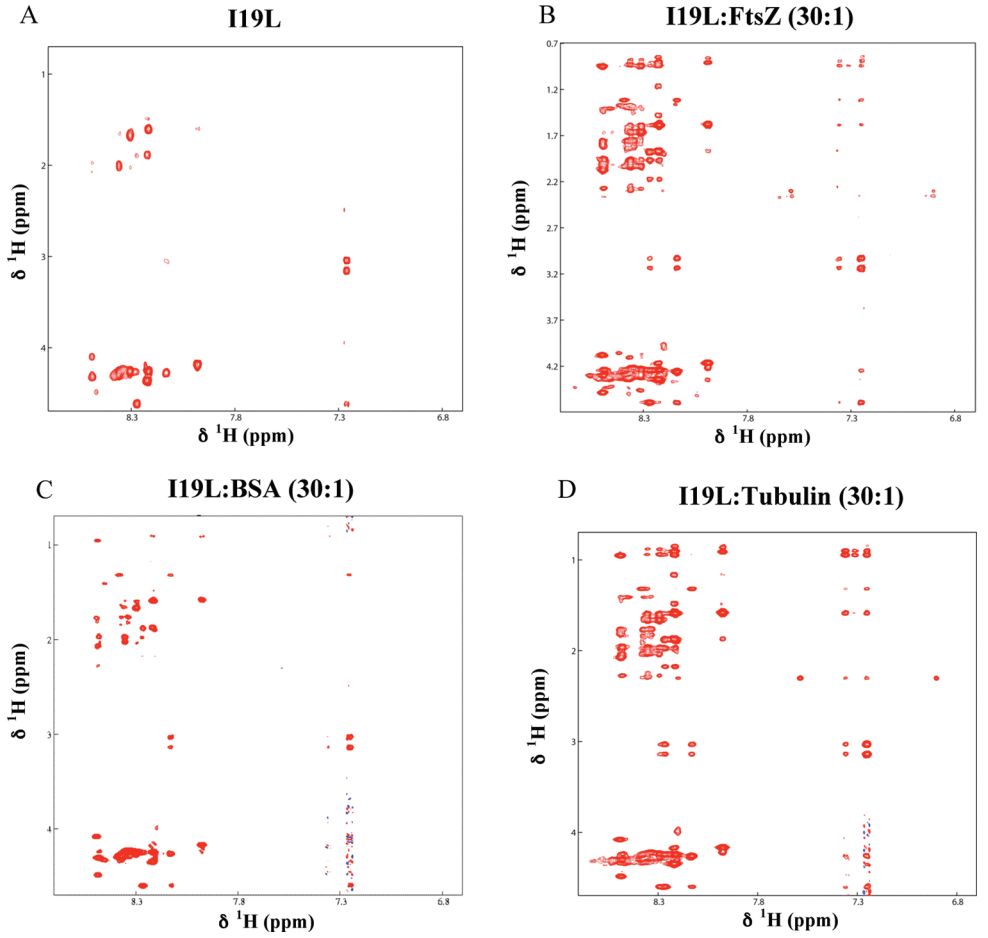

FIGURE 3: Amide region of NOESY spectra: (A) I19L (1 mM), (B) I19L (1 mM) in the presence of FtsZ (30 μM), (C) I19L (1 mM) in the presence of BSA (30 μM), and (D) I19L (1 mM) in the presence of tubulin (30 μM).

Table 1: Structural Statistics for the 40 Best Conformers Calculated for I19L

no. of distance restraints	
intraresidue ($i - j = 0$)	143
sequential ($i - j = 1$)	69
medium-range ($2 \leq i - j \leq 4$)	16
long-range ($i - j > 4$)	15
total	243
no. of distance violations of > 1 Å	0
rmsd[a] values from idealized covalent geometry	
bonds (Å)	0.0084 ± 0.0003
angles (deg)	0.91 ± 0.04
impropers (deg)	0.81 ± 0.07
Ramachandran plot (%)	
most favored regions	55
additionally allowed regions	32
mean pairwise rmsd[a] values (Å) for all residues	0.91 ± 0.7, 1.83 ± 0.92

[a]Root-mean-square deviation.

these reasons, this structure has not been considered as a probable conformation. In the two remaining I19L−FtsZm structures (second and eighth), the peptide interacts with and extends the β sheet of the C-terminal domain (Figure 6), in both cases in a manner very similar to what was found for the I19L−tubulin complex. Nevertheless, with regard to the distances between I19L residues I1, L6, F15, L17, and L19 and the protein (see Table 2 of the Supporting Information), one can observe that the last four residues have a minimal distance between 4 and 7 Å, whereas the I1 amino acid is more than 11 Å from the protein.

DISCUSSION

FtsZ is a critical protein for prokaryotic cell division. The need for new drug candidates for the development of new antibiotics is undisputed, especially in the context of antibiotic resistance (*56*). FtsZ is a target particularly suited to inhibit bacterial growth. Understanding the interactions of FtsZ with ligands and differences and similarities between FtsZ and tubulin for ligand binding appears to be a fundamental step in ascertaining specificity. We demonstrated that peptides derived from the N-terminal region of stathmin are able to impede tubulin polymerization (*34*). The aim of this work was thus to study the effect of I19L, the most efficient of these peptides, on FtsZ assembly.

We first report that the I19L peptide binds to FtsZ, as reported for tubulin. Indeed, I19L was found in the 25000*g* sedimentation pellet after FtsZ polymerization (Figure 1D) or bundling, and STD-NMR experiments (Figure 2) show the direct interaction of I19L with FtsZ. In addition, we found that I19L affects the bundling of FtsZ (Figure 1C) as reported earlier for two different FtsZ inhibitors: sanguinarine (*20*) and EzrA (*28*).

The β Hairpin Folds of I19L Interacting with FtsZ or Tubulin Present Some Differences. We showed here that the I19L peptide, while disordered in solution (*34*), folds when interacting with FtsZ. Its bound structure consists of two extended strands, as observed when I19L interacts with tubulin. The presence of such extended strands is consistent with predictions of Eswar et al. (*55*), which show that the propensity of amino acids 2−6 and 14−18 to fold in an extended strand conformation

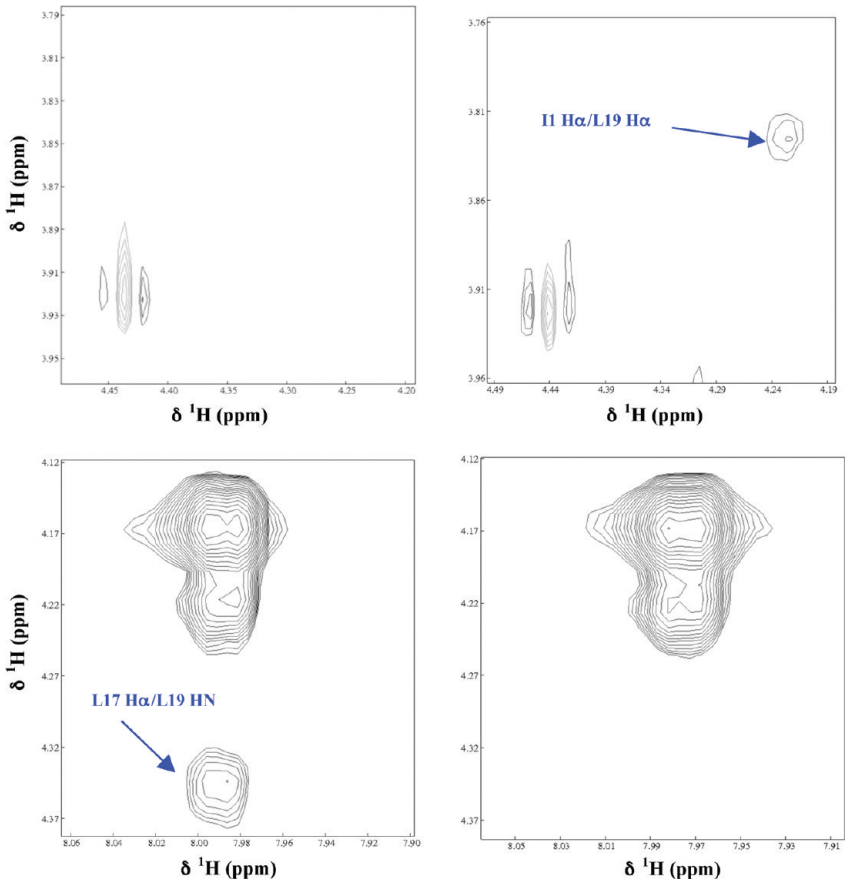

FIGURE 4: Region of the TRNOESY spectra of I19L (1 mM) in interaction with FtsZ (30 μM) (left) and I19L (1 mM) with tubulin (30 μM) (right).

is superior to 1. In addition, a BLAST similarity query shows that I19L has significant sequence similarities (47% identical and 80% homologous) with a subdomain of L22 (ribosomal protein of *Nicotiana tomentosiformis*, amino acid residues 86−104, YP_398904), which interestingly is also composed of two strands [Protein Data Bank (PDB) entry 1BXE]. However, the long-range nOes (presence or intensities) observed in the I19L−tubulin interaction are not identical to those observed in the I19L−FtsZ interaction. Moreover, nOes characteristic of the β hairpin fold were not found in the FtsZ−I19L complex. This explains the differences observed between the structures of I19L calculated from the I19L−tubulin and I19L−FtsZ interactions (Figure 5C).

The Mechanisms of Interaction of I19L with FtsZ and Tubulin Are Different. It has been proposed that FtsZ is the bacterial ancestor (for a review, see ref *57*). Though FtsZ and tubulin have a low level of sequence similarity, they exhibit very similar three-dimensional structures (*3*). Some compounds, active on tubulin, have been tested to see if they could also target prokaryotic cell division [as thiabendazole (*58*)]. In this context, I19L could be the first example of a peptide that could bind both tubulin and FtsZ.

However, the STD experiments presented here show that the mechanisms of interaction of I19L with FtsZ and tubulin are different, though the general overall folding of I19L looks similar in these two cases. Indeed, in the I19L−tubulin interaction, all residues of I19L in contact with tubulin were located on the same β2 strand [14, 15, 17, and 19 (*34*)], whereas residues from both strands are involved in this contact in the case of the I19L−FtsZ interaction (residues 1, 6, 15, and 17/19). Some hydrophobic residues (L17/19 and F15) from I19L, however, participate to the binding with both FtsZ and tubulin.

I19L May Interact with FtsZ at Two Potential Binding Sites. One possible site for binding of I19L to FtsZ could be near the GTP binding pocket, showing electrostatic interactions as proposed by docking calculations (Figure 6E). In this case, the STD data could be fitted with an interaction between I19L and FtsZ residues located in the GTP binding pocket [R78, E168, and R169 (Table 1 of the Supporting Information)]. Interestingly, MciZ, a 40-amino acid peptide recently demonstrated to inhibit cytokinesis and to interact strongly with FtsZ (*31*), presents a partial sequence similarity with I19L in its N-terminal portion (27.3% identical), but secondary structure predictions show that the amino acids which superimpose with I19L on its N-terminal region may also adopt a β sheet fold (Figure 7). Though the binding site of MciZ on FtsZ was not fully described, it was shown that a mutation of FtsZ in the GTP binding pocket affects the MciZ−FtsZ interaction which reinforces the proposal that I19L may interact also at this location. On the other hand, an interaction of I19L with FtsZ in a site similar to that observed when it interacts with tubulin cannot be excluded. According to this latter model (*34*), I19L binds a hydrophobic pocket located on α-tubulin at the interdimer interface between helix H10 and β strand S9 and extends the tubulin intermediate β sheet domain. We thus attempted to dock the I19L peptide near this site on FtsZ but observed that the T7 loop in all structures may impede I19L binding if the loop is not flexible. To examine more closely the possibility of such an interaction, we aligned the secondary structures of 12 FtsZ structures extracted from diverse organisms (*Mycobacterium*, *Methanococcus*, *Pseudomonas*, and *Bacillus subtilis*). In all structures, a T7 loop was

present but always very poorly defined which strengthens the idea that it is flexible.

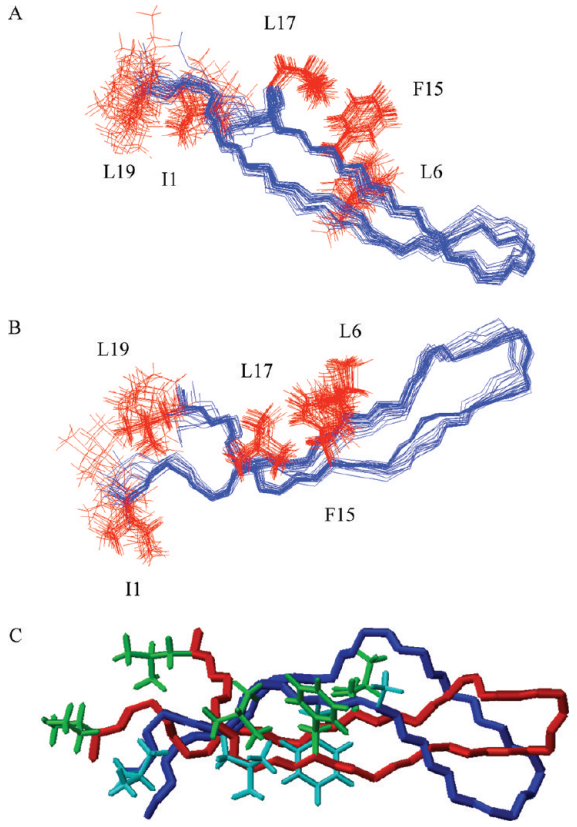

FIGURE 5: (A and B) Two different representations of the NMR solution structure of I19L in interaction with FtsZ. Lateral side chains of amino acids in contact with FtsZ derived from 1D STD NMR experiments are highlighted. (C) Overlay representation of the lowest-energy structures of I19L bound to FtsZ (Cα backbone, red; interacting side chains, green) and to tubulin (Cα backbone, blue; interacting side chains, cyan).

The loop of FtsZ is quite homologuous to the T7 loop of tubulin [28% identical sequence and 57% homologous sequence (Figure 8)]. In the case of tubulin, it has been shown that loop T7 is very flexible. For example, in the complex with RB3 (PDB entry 1sa0), the T7 loop of tubulin has a different conformation than in zinc sheets (PDB entry 1tub). Similarly, we cannot exclude the possibility that the T7 loop of FtsZ may change its conformation in the presence of I19L. Results of the docking calculations of I19L with FtsZd in which the loop T7 was partially deleted show that the interaction of I19L with the β sheet of the C-terminal domain is indeed one of the most favorable (Figure 6F). In that case, the STD-NMR data obtained here could be explained by the proximity of I19L to FtsZ residues P313, N314, and/or W319. However, in the second and eighth docked I19L−FtsZd structures, I19L residue I1 seems quite distant from FtsZ which is inconsistent with STD-NMR data. This putative binding pocket appears thus less probable than the GTP pocket.

I19L Seems To Influence FtsZ Bundling Induced by Calcium. It has already been shown that the nature of FtsZ bundles could be strongly dependent on buffer conditions (*59*). Beuria et al. (*24*) reported strong differences in the light scattering spectra when glutamate was used instead of calcium, which was interpreted as the result of thicker bundles or due to different mechanisms of FtsZ polymerization. Marrington et al. (*60*) discussed changes in bundles due to Mg^{2+} and Ca^{2+} and showed that FtsZ bundling is linked to a conformational change in bound GTP. Here, we propose that the bundles observed in the presence of I19L and calcium are quite different from those observed with calcium alone. It has been demonstrated that the conformation of the nucleotide influences the polymerization and bundling of FtsZ. The structure of the filaments adopts a straight or curved conformation when bound to GTP or GDP (*61*). Small and co-workers (*62*) showed that FtsZ bundling by YgfE involves a conformational change in bound GTP. By combining STD-NMR data with molecular docking calculations, we show here

Table 2: List of the Lowest-Energy Structures of the Docked Complexes of I19L with Wild-Type FtsZ and Deleted Versions[a]

Rank	I19L-FtsZw (kJ/mol)	Occurrence	Averaged minimal distance (Å)		I19L-FtsZd (kJ/mol)	Occurrence	Averaged minimal distance (Å)
1	-320.7	4	7.05	↔	-320.5	10	7.06
2	-314.7	4	5.20	↘	-320.4*	8	6.54
3	-313.6	7	7.09	↔	-314.8	1	5.23
4	-308.5	9	7.61	↘	-313.6	3	7.07
5	-305.5	14	6.48	↔	-308.3	6	7.53
6	-302.2	7	9.38	↘	-305.6	6	6.44
7	-301.7	11	5.06		-303.3*	16	6.22
8	-301.4*	5	5.75		-302.6*	9	6.57

[a]The arrows show the correspondence of the models. The average minimal distances between peptide residues I1, L6, F15, L17, and L19 and the nearest residues of FtsZ were calculated.

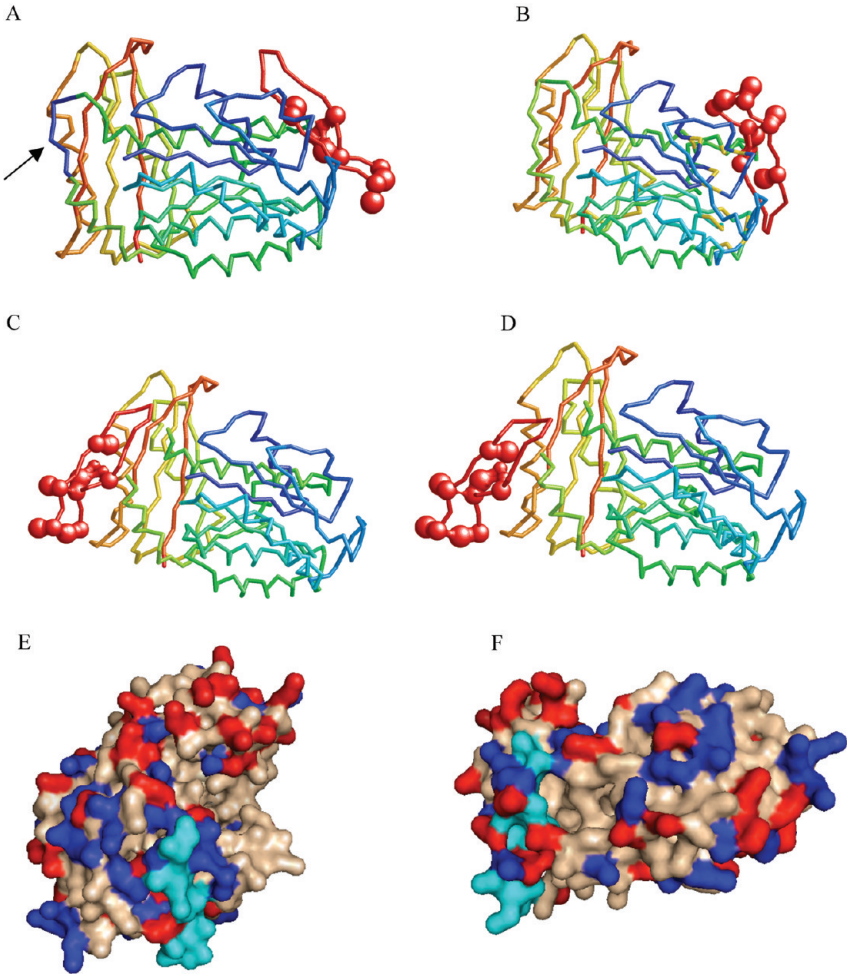

FIGURE 6: Docking models of the I19L−FtsZ complex. (A) Model 5 of the I19L−FtsZw complex. The part of the T7 loop that is colored blue (arrow) was deleted in FtsZd. (B) Model 7 of the I19L−FtsZw complex. (C) Model 2 of the I19L−FtsZd complex. (D) Model 8 of the I19L−FtsZd complex. (E) Electrostatic and hydrophobic surface representation of model 5 of the I19L−FtsZw complex. (F) Electrostatic and hydrophobic surface representation of model 2 of the I19L−FtsZd complex. In panels A−D, grains corresponding to the I19L side chains in interaction with FtsZ according to STD-NMR experiments are depicted as red spheres.

```
A)                          10         20         30         40
                            |          |          |          |
MciZ(B. Cereus)     MKVYILPNRVTLVGKAWQIRHKLKQYSKEYTTVQEWITANKVKH
                    ..:  :  :..  :.:...
I19L                IQVKELEKRAS--GQAFELIL----------------------
                            10

 B)             10         20         30         40
                |          |          |          |
UNK_5137MKVYILPNRVTLVGKAWQIRHKLKQYSKEYTTVQEWITANKVKH
PHD        ceeeeeccceeeeechhhhhhhhhhhcccchhhhhhhhhcccc
```

FIGURE 7: (A) Alignment of I19L and MciZ sequences. (B) Prediction structure of MciZ (*64*).

```
Tubulin(human)      239 TASLRFDGALNVDL
FtsZ(Coli)          197 AELITRPGLMNVDF
FtsZ(M. Jannaschii) 223 VELITKDGLINVDF
```

FIGURE 8: Sequence alignment of T7 loops.

that the most probable interaction site of I19L on FtsZ is the GTP site. Consequently, I19L could be responsible for the formation of bundles which diffract less than regular FtsZ ones.

In conclusion, we show here for the first time that a short peptide that impedes tubulin polymerization is also able to modify FtsZ assembly dynamics. The data, however, strongly suggest that the binding of I19L to FtsZ differs from its interaction with tubulin, which may be related to the evolutionary distance between these two homologue proteins. The results may be of use in the development of specific small molecules to target FtsZ for novel antimicrobial strategies.

ACKNOWLEDGMENT

We thank Pr. D. Panda (ITT Bombay) who provided the FtsZ plasmid and whose help has been essential for this project. We thank David Pastré (U829) for fruitful discussions.

SUPPORTING INFORMATION AVAILABLE

Minimal distances between I19L and FtsZ for five models and STD control experiments. This material is available free of charge via the Internet at http://pubs.acs.org.

REFERENCES

1. Errington, J., Daniel, R. A., and Scheffers, D. J. (2003) Cytokinesis in bacteria. *Microbiol. Mol. Biol. Rev. 67*, 52–65 (table).
2. Vollmer, W. (2006) The prokaryotic cytoskeleton: A putative target for inhibitors and antibiotics? *Appl. Microbiol. Biotechnol. 73*, 37–47.
3. Lowe, J., and Amos, L. A. (1998) Crystal structure of the bacterial cell-division protein FtsZ. *Nature 391*, 203–206.
4. Nogales, E., Wolf, S. G., and Downing, K. H. (1998) Structure of the $\alpha\beta$ tubulin dimer by electron crystallography. *Nature 391*, 199–203.

5. Nogales, E., and Wang, H. W. (2006) Structural mechanisms underlying nucleotide-dependent self-assembly of tubulin and its relatives. *Curr. Opin. Struct. Biol. 16*, 221–229.
6. Nogales, E., Downing, K. H., Amos, L. A., and Lowe, J. (1998) Tubulin and FtsZ form a distinct family of GTPases. *Nat. Struct. Biol. 5*, 451–458.
7. Oliva, M. A., Cordell, S. C., and Lowe, J. (2004) Structural insights into FtsZ protofilament formation. *Nat. Struct. Mol. Biol. 11*, 1243–1250.
8. Scheffers, D. J., de Wit, J. G., den Blaauwen, T., and Driessen, A. J. (2002) GTP hydrolysis of cell division protein FtsZ: Evidence that the active site is formed by the association of monomers. *Biochemistry 41*, 521–529.
9. Lowe, J., Li, H., Downing, K. H., and Nogales, E. (2001) Refined structure of $\alpha\beta$-tubulin at 3.5 Å resolution. *J. Mol. Biol. 313*, 1045–1057.
10. Huzil, J. T., Chik, J. K., Slysz, G. W., Freedman, H., Tuszynski, J., Taylor, R. E., Sackett, D. L., and Schriemer, D. C. (2008) A unique mode of microtubule stabilization induced by peloruside A. *J. Mol. Biol. 378*, 1016–1030.
11. Nicolaou, K. C., Winssinger, N., Pastor, J., Ninkovic, S., Sarabia, F., He, Y., Vourloumis, D., Yang, Z., Li, T., Giannakakou, P., and Hamel, E. (1997) Synthesis of epothilones A and B in solid and solution phase. *Nature 387*, 268–272.
12. Cormier, A., Marchand, M., Ravelli, R. B., Knossow, M., and Gigant, B. (2008) Structural insight into the inhibition of tubulin by vinca domain peptide ligands. *EMBO Rep. 9*, 1101–1106.
13. Zhou, J., and Giannakakou, P. (2005) Targeting microtubules for cancer chemotherapy. *Curr. Med. Chem. Anticancer Agents 5*, 65–71.
14. Ravelli, R. B. G., Gigant, B., Curmi, P. A., Jourdain, I., Lachkar, S., Sobel, A., and Knossow, M. (2004) Insight into tubulin regulation from a complex with colchicine and a stathmin-like domain. *Nature 428*, 198–202.
15. Lappchen, T., Hartog, A. F., Pinas, V. A., Koomen, G. J., and den Blaauwen, T. (2005) GTP analogue inhibits polymerization and GTPase activity of the bacterial protein FtsZ without affecting its eukaryotic homologue tubulin. *Biochemistry 44*, 7879–7884.
16. Domadia, P., Swarup, S., Bhunia, A., Sivaraman, J., and Dasgupta, D. (2007) Inhibition of bacterial cell division protein FtsZ by cinnamaldehyde. *Biochem. Pharmacol. 74*, 831–840.
17. Haydon, D. J., Stokes, N. R., Ure, R., Galbraith, G., Bennett, J. M., Brown, D. R., Baker, P. J., Barynin, V. V., Rice, D. W., Sedelnikova, S. E., Heal, J. R., Sheridan, J. M., Aiwale, S. T., Chauhan, P. K., Srivastava, A., Taneja, A., Collins, I., Errington, J., and Czaplewski, L. G. (2008) An inhibitor of FtsZ with potent and selective anti-staphylococcal activity. *Science 321*, 1673–1675.
18. Yu, X. C., and Margolin, W. (1998) Inhibition of assembly of bacterial cell division protein FtsZ by the hydrophobic dye 5,5′-bis-(8-anilino-1-naphthalenesulfonate). *J. Biol. Chem. 273*, 10216–10222.
19. Lopus, M., and Panda, D. (2006) The benzophenanthridine alkaloid sanguinarine perturbs microtubule assembly dynamics through tubulin binding. A possible mechanism for its antiproliferative activity. *FEBS J. 273*, 2139–2150.
20. Beuria, T. K., Santra, M. K., and Panda, D. (2005) Sanguinarine blocks cytokinesis in bacteria by inhibiting FtsZ assembly and bundling. *Biochemistry 44*, 16584–16593.
21. Yu, X. C., and Margolin, W. (1997) Ca^{2+}-mediated GTP-dependent dynamic assembly of bacterial cell division protein FtsZ into asters and polymer networks in vitro. *EMBO J. 16*, 5455–5463.
22. Weisenberg, R. C. (1972) Microtubule formation in vitro in solutions containing low calcium concentrations. *Science 177*, 1104–1105.
23. Hamel, E., and Lin, C. M. (1981) Glutamate-induced polymerization of tubulin: Characteristics of the reaction and application to the large-scale purification of tubulin. *Arch. Biochem. Biophys. 209*, 29–40.
24. Beuria, T. K., Krishnakumar, S. S., Sahar, S., Singh, N., Gupta, K., Meshram, M., and Panda, D. (2003) Glutamate-induced assembly of bacterial cell division protein FtsZ. *J. Biol. Chem. 278*, 3735–3741.
25. Lappchen, T., Pinas, V. A., Hartog, A. F., Koomen, G. J., Schaffner-Barbero, C., Andreu, J. M., Trambaiolo, D., Lowe, J., Juhem, A., Popov, A. V., and den Blaauwen, T. (2008) Probing FtsZ and tubulin with C8-substituted GTP analogs reveals differences in their nucleotide binding sites. *Chem. Biol. 15*, 189–199.
26. Wang, X., Huang, J., Mukherjee, A., Cao, C., and Lutkenhaus, J. (1997) Analysis of the interaction of FtsZ with itself, GTP, and FtsA. *J. Bacteriol. 179*, 5551–5559.
27. Mosyak, L., Zhang, Y., Glasfeld, E., Haney, S., Stahl, M., Seehra, J., and Somers, W. S. (2000) The bacterial cell-division protein ZipA and its interaction with an FtsZ fragment revealed by X-ray crystallography. *EMBO J. 19*, 3179–3191.
28. Singh, J. K., Makde, R. D., Kumar, V., and Panda, D. (2007) A membrane protein, EzrA, regulates assembly dynamics of FtsZ by interacting with the C-terminal tail of FtsZ. *Biochemistry 46*, 11013–11022.
29. Singh, J. K., Makde, R. D., Kumar, V., and Panda, D. (2008) SepF increases the assembly and bundling of FtsZ polymers and stabilizes FtsZ protofilaments by binding along its length. *J. Biol. Chem. 283*, 31116–31124.
30. Ishikawa, S., Kawai, Y., Hiramatsu, K., Kuwano, M., and Ogasawara, N. (2006) A new FtsZ-interacting protein, YlmF, complements the activity of FtsA during progression of cell division in *Bacillus subtilis*. *Mol. Microbiol. 60*, 1364–1380.
31. Handler, A. A., Lim, J. E., and Losick, R. (2008) Peptide inhibitor of cytokinesis during sporulation in *Bacillus subtilis*. *Mol. Microbiol. 68*, 588–599.
32. Dajkovic, A., Lan, G., Sun, S. X., Wirtz, D., and Lutkenhaus, J. (2008) MinC spatially controls bacterial cytokinesis by antagonizing the scaffolding function of FtsZ. *Curr. Biol. 18*, 235–244.
33. Cordell, S. C., Robinson, E. J., and Lowe, J. (2003) Crystal structure of the SOS cell division inhibitor SulA and in complex with FtsZ. *Proc. Natl. Acad. Sci. U.S.A. 100*, 7889–7894.
34. Clement, M. J., Jourdain, I., Lachkar, S., Savarin, P., Gigant, B., Knossow, M., Toma, F., Sobel, A., and Curmi, P. A. (2005) N-Terminal stathmin-like peptides bind tubulin and impede microtubule assembly. *Biochemistry 44*, 14616–14625.
35. Rivas, G., Lopez, A., Mingorance, J., Ferrandiz, M. J., Zorrilla, S., Minton, A. P., Vicente, M., and Andreu, J. M. (2000) Magnesium-induced linear self-association of the FtsZ bacterial cell division protein monomer. The primary steps for FtsZ assembly. *J. Biol. Chem. 275*, 11740–11749.
36. Lu, C., Stricker, J., and Erickson, H. P. (1998) FtsZ from *Escherichia coli*, *Azotobacter vinelandii*, and *Thermotoga maritima*: Quantitation, GTP hydrolysis, and assembly. *Cell Motil. Cytoskeleton 40*, 71–86.
37. Rance, M., Sorensen, O. W., Bodenhausen, G., Wagner, G., Ernst, R. R., and Wuthrich, K. (1983) Improved spectral resolution in cosy ^{1}H NMR spectra of proteins via double quantum filtering. *Biochem. Biophys. Res. Commun. 117*, 479–485.
38. Braunschweiler, L., and Ernst, R. R. (1983) Coherence transfer by isotropic mixing: Application to proton correlation spectroscopy. *J. Magn. Reson. 53*, 521–528.
39. Kumar, A., Ernst, R. R., and Wüthrich, K. (1980) A two-dimensional nuclear Overhauser enhancement (2D NOE) experiment for the elucidation of complete proton-proton cross-relaxation networks in biological macromolecules. *Biochem. Biophys. Res. Commun. 95*, 1–6.
40. Bax, A., and Davies, D. G. (1985) Practical aspects of two-dimensional transverse NOE spectroscopy. *J. Magn. Reson. 63*, 207–213.
41. Bax, A., and Davies, D. G. (1985) MLEV-17-based two-dimensional homonuclear magnetization transfer spectroscopy. *J. Magn. Reson. 65*, 355–360.
42. Clore, G. M., and Gronenborn, A. M. (1982) Theory and applications of the transferred nuclear Overhauser effect to the study of the conformations of small ligands bound to proteins. *J. Magn. Reson. 48*, 402–417.
43. Clore, G. M., and Gronenborn, A. M. (1983) Theory of the time dependent transferred nuclear Overhauser effect: Application to the structural analysis of ligand-protein complexes in solution. *J. Magn. Reson. 53*, 423–442.
44. Mayer, M., and Meyer, B. (1999) Characterization of Ligand Binding by Saturation Transfer Difference NMR Spectra. *Angew. Chem., Int. Ed. 35*, 1784–1788.
45. Piotto, M., Saudek, V., and Sklenar, V. (1992) Gradient-tailored excitation for single-quantum NMR spectroscopy of aqueous solutions. *J. Biomol. NMR 2*, 661–665.
46. Johnson, B. A., and Blevins, R. A. (1994) NMRView: A Computer Program for the Visualization and Analysis of NMR Data. *J. Biomol. NMR 4*, 603–614.
47. Baleja, J., Moult, J., and Sykes, B. D. (1990) Distance measurement and structure refinement with NOE data. *J. Magn. Reson. 87*, 375–384.
48. Brünger, A. T., Adams, P. D., Clore, G. M., DeLano, W. L., Gros, P., Grosse-Kunstleve, R. W., Jiang, J. S., Kuszewski, J., Nilges, M., and Pannu, N. S.; et al. (1998) Crystallography and NMR system: A new software suite for macromolecular structure determination. *Acta Crystallogr. D54*, 905–921.

49. Laskowski, R. A., MacArthur, M. W., Moss, D. A., and Thornton, J. M. (1993) PROCHECK: A program to check the stereochemical quality of protein structures. *J. Appl. Crystallogr. 26*, 283–291.
50. Koradi, R., Billeter, M., and Wüthrich, K. (1996) MOLMOL: A program for display and analysis of macromolecular structures. *J. Mol. Graphics 14*, 51–55.
51. Basdevant, N., Borgis, D., and Ha-Duong, T. (2007) A coarse-grained protein-protein potential derived from an all-atom force field. *J. Phys. Chem. B 111*, 9390–9399.
52. Zacharias, M. (2005) ATTRACT: Protein-protein docking in CAPRI using a reduced protein model. *Proteins 60*, 252–256.
53. Cornell, W. D., Cieplak, P., Bayly, C. I., Gould, I. R., Merz, K. M., Ferguson, D. M., Spellmeyer, D. C., Fox, T., Caldwell, J. W., and Kollman, P. A. (1995) A second generation force field for the simulation of proteins, nucleic acids and organic molecules. *J. Am. Chem. Soc. 117*, 5179–5197.
54. Hingerty, B. E., Ritchie, R. H., Ferrell, T. L., and Turner, J. E. (1985) Dielectric effects in biopolymers: The theory of ionic saturation revisited. *Biopolymers 24*, 427–439.
55. Eswar, N., Ramakrishnan, C., and Srinivasan, N. (2003) Stranded in isolation: Structural role of isolated extended strands in proteins. *Protein Eng. 16*, 331–339.
56. Payne, D. J. (2008) Microbiology. Desperately seeking new antibiotics. *Science 321*, 1644–1645.
57. van den, E. F., Amos, L., and Lowe, J. (2001) Bacterial ancestry of actin and tubulin. *Curr. Opin. Microbiol. 4*, 634–638.
58. Sarcina, M., and Mullineaux, C. W. (2000) Effects of tubulin assembly inhibitors on cell division in prokaryotes in vivo. *FEMS Microbiol. Lett. 191*, 25–29.
59. Kuchibhatla, A., Rasheed, A. S., Narayanan, J., Bellare, J., and Panda, D. (2009) An Analysis of FtsZ Assembly Using Small Angle X-ray Scattering and Electron Microscopy. *Langmuir 25*, 3775–3785.
60. Marrington, R., Small, E., Rodger, A., Dafforn, T. R., and Addinall, S. G. (2004) FtsZ fiber bundling is triggered by a conformational change in bound GTP. *J. Biol. Chem. 279*, 48821–48829.
61. Lu, C., Reedy, M., and Erickson, H. P. (2000) Straight and curved conformations of FtsZ are regulated by GTP hydrolysis. *J. Bacteriol. 182*, 164–170.
62. Small, E., Marrington, R., Rodger, A., Scott, D. J., Sloan, K., Roper, D., Dafforn, T. R., and Addinall, S. G. (2007) FtsZ polymer-bundling by the *Escherichia coli* ZapA orthologue, YgfE, involves a conformational change in bound GTP. *J. Mol. Biol. 369*, 210–221.
63. Hamon, L., Panda, D., Savarin, P., Joshi, V., Bernhard, J., Mucher, E., Mechulam, A., Curmi, P. A., and Pastre, D. (2009) Mica surface promotes the assembly of cytoskeletal proteins. *Langmuir 25*, 3331–3335.
64. Rost, B., Yachdav, G., and Liu, J. (2004) The PredictProtein Server. *Nucleic Acids Res. 32* (Web Server issue), W321–W326.